Power Electronic Systems
Laboratory

IEEE Transactions on Industry Applications, Vol. 51, No. 5, pp. 4100-4110, September/October 2015

Novel Principle for Flux Sensing in the Application of a DC + AC Current Sensor

L. Schrittwieser,
M. Mauerer,
D. Bortis,
G. Ortiz,
J.W.Kolar

Eidgenössische Technische Hochschule Zürich
Swiss Federal Institute of Technology Zurich

Novel Principle for Flux Sensing in the Application of a DC + AC Current Sensor

Lukas Schrittwieser, *Student Member, IEEE*, Mario Mauerer, *Student Member, IEEE*, Dominik Bortis, *Member, IEEE*, Gabriel Ortiz, *Member, IEEE*, and Johann W. Kolar, *Fellow, IEEE*

***Abstract*—This paper presents a new concept for measuring DC and AC magnetic flux densities within a ferromagnetic material. It is based on a measurement of the material's magnetostriction, which is its relative change in length due to the magnetic flux density inside the material. This dimensional change is converted to an electrical signal using a piezoelectric strain sensor. An additional sinusoidal AC excitation of the core material provides higher sensitivity of the length measurement and overcomes the inherent high-pass characteristic of the piezoelectric sensor. Therefore, flux density signals from DC to the kilohertz range can be measured. The concept's feasibility is demonstrated with the design and implementation of an isolated DC + AC current sensor with a measurement range of ± 20 A and a bandwidth from DC to 20 MHz.**

***Index Terms*—Current measurement, DC flux density, magnetic field measurement, magnetic variable control, magnetomechanical effects, magnetostriction, piezo film sensor.**

I. Introduction

A precise and high-bandwidth current measurement is a mandatory requirement of many modern power electronic converters and power distribution systems. It enables, for example, the implementation of high-performance current control loops and a safe shutdown in case the maximum allowed current value is exceeded. Depending on the specific application and the required performance of the sensor, the existing current measurement concepts can be classified according to their key operating principles. Fig. 1 gives an overview of the most common current measurement methods utilized in power electronics. Their key features are presented in the following.

A. Nonisolated Current Measurement Concepts

If no galvanic isolation between the input current and the sensing circuit is required, the current can be directly measured with a shunt resistor [1]. To achieve a high bandwidth of several tens of megahertz or more, special construction techniques for the shunt are required to reduce parasitic effects [2]. While shunt-based current sensors are straightforward to implement, achieve high bandwidths, and have a low component count, a tradeoff between output signal to noise ratio and power losses exists. Furthermore, as the shunt resistor is a passive element, these losses are covered by the circuit under test, which results in lower efficiency of the power conversion.

B. Isolated AC Measurement Concepts

When galvanic isolation between the current to be measured and the sensor is required, the measurement principle is typically based on *Ampère's Law* and *Faraday's Law of induction*, i.e., effects caused by the magnetic field of the current, are exploited. There, Rogowski coils or AC current transformers (CTs) are commonly used if only AC currents need to be measured, e.g., in transmission systems [3], [4]. Typically, CTs consist of just two components: a transformer and a burden resistor, as shown in Fig. 2(a). The transformer provides galvanic isolation and reduces the input current to a value that can be measured with low losses using the burden resistor. As the transformer's magnetizing inductance effectively bypasses the burden resistor for low frequencies, CTs show a high-pass characteristic with a lower cutoff frequency ω_{ct}. While simplicity is their main advantage, the transformer's core material introduces a nonlinearity due to a nonlinear increase of the magnetizing current required for increasing excitation and/or saturation. This can be a significant disadvantage, e.g., in the protection of power systems [5], [6].

Since Rogowski coils are wound around a nonmagnetic core, they show a much better linearity than AC CTs. The coil can be wound on a flexible material, and it can be opened, which allows an easy installation around power conductors. However, the mutual inductance between the primary conductor, carrying the current to be measured, and the measurement winding is much smaller compared with a CT. Consequently, the output signal of the coil is much lower than that of a CT. Instead of a burden resistor, an integrator circuit is used to amplify the signal and to reconstruct the measured current's shape. Inevitable offset errors require the use of high-pass filters that limit the lower frequency at which Rogowski coils can be operated with sufficient precision [7].

C. Open-Loop DC + AC Current Measurement Concepts

If AC and DC components need to be captured, a magnetic flux sensor is used to measure the flux density originating from the measured current $i_{\mathrm{m}}(t)$. As the bandwidth of these

Manuscript received August 21, 2014; revised January 15, 2015; accepted April 16, 2015. Date of publication May 18, 2015; date of current version September 16, 2015. Paper 2014-PEDCC-0585.R1, presented at the 2014 International Power Electronics Conference (IPEC-Hiroshima 2014 ECCE-Asia), Hiroshima, Japan, May 18–21, and approved for publication in the IEEE TRANSACTIONS ON INDUSTRY APPLICATIONS by the Power Electronic Devices and Components Committee of the IEEE Industry Applications Society.

The authors are with the Power Electronic Systems Laboratory, ETH Zurich, 8092 Zurich, Switzerland (e-mail: schrittwieser@lem.ee.ethz.ch; mauerer@lem.ee.ethz.ch; bortis@lem.ee.ethz.ch; ortiz@lem.ee.ethz.ch; kolar@lem.ee.ethz.ch).

Color versions of one or more of the figures in this paper are available online at http://ieeexplore.ieee.org.

Digital Object Identifier 10.1109/TIA.2015.2434875

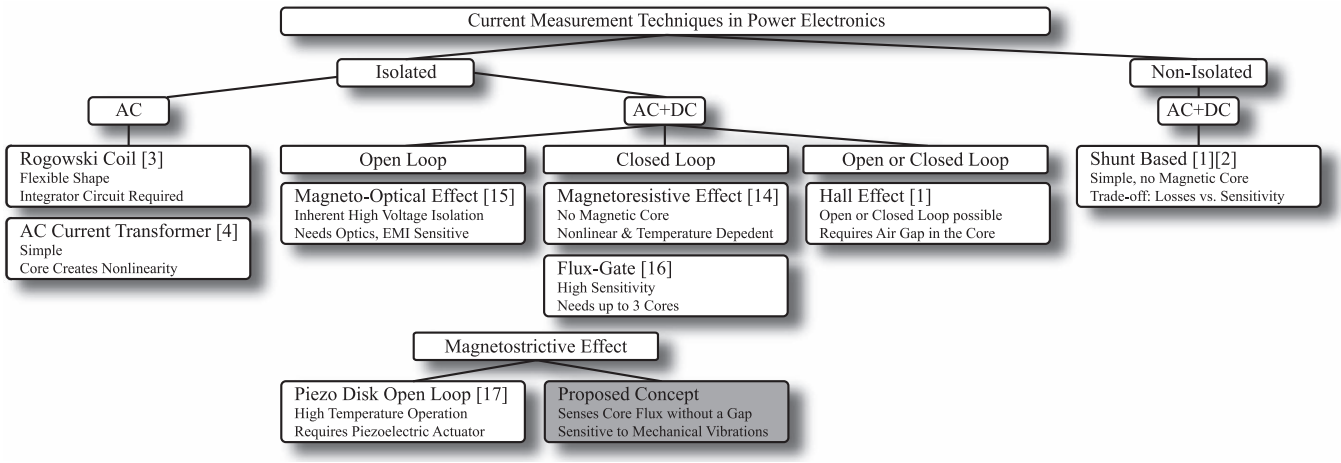

Fig. 1. Overview of previously presented current measurement technologies utilized in power electronic systems.

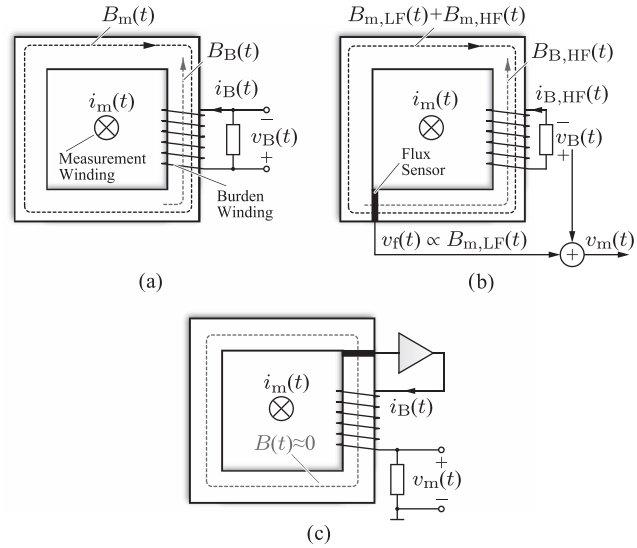

Fig. 2. Current transducer concepts. (a) CT, usable for AC currents only. (b) Flux sensor is inserted in the magnetic path to measure the low-frequency component of i_{m}. Its output signal is added to the CT's output voltage that measures the high-frequency components. (c) Active low-frequency flux compensation using an additional power amplifier that creates low-frequency components in $i_{\mathrm{B}}(t)$ in order to reduce the core flux $B(t)$ close to zero for frequencies below ω_{ct}.

flux sensors is typically not sufficient for a high-performance current sensor, they are combined with a CT as shown in Fig. 2(b). The CT's core is typically gapped in order to insert a flux sensor, e.g., a Hall element, into its magnetic path.

Note that no fine-tuned frequency matching is required between the CT's high-pass cutoff frequency ω_{ct} and the flux sensor's low-pass cutoff frequency. All frequency components of the input current $i_{\mathrm{m}}(t)$, which are above ω_{ct}, cause a current flow in the burden resistor, which in turn creates a flux density signal $B_{\mathrm{B,HF}}(t)$ in the core. This cancels the core flux components $B_{\mathrm{m,HF}}(t)$ caused by the high-frequency components of $i_{\mathrm{m}}(t)$. Consequently, only the low-frequency components $B_{\mathrm{m,LF}}(t)$ remain in the core and need to be measured by the flux sensor [8]. Adding the output signals of the CT and the flux sensor yields the sensor output $v_{\mathrm{m}}(t)$, which is proportional to $i_{\mathrm{m}}(t)$.

A specially dimensioned CT is required for this concept because the core material provides the magnetic path, which concentrates the magnetic field to the flux sensor. Any nonlinearity of the core material will degrade the sensor's performance. Furthermore, open-loop sensors are typically sensitive to gain variations of the flux sensor, e.g., due to production tolerances or temperature dependences. These disadvantages can be overcome by using a closed-loop sensor principle, as shown in Fig. 2(c) and as explained in the following.

D. Closed-Loop DC + AC Current Measurement Concepts

In a closed-loop sensor, an amplifier circuit is added as shown in Fig. 2(c). It is used to control the current $i_{\mathrm{B}}(t)$ through the burden winding in such a way that the signal measured by the flux sensor is ideally zero. Then, $i_{\mathrm{B}}(t)$ is proportional to the measured current $i_{\mathrm{m}}(t)$ [9], [10]. The constant of proportionality is defined by the turns ratio of the measurement and burden windings.

With this configuration, frequency components $i_{\mathrm{m,HF}}(t)$ above the CT's lower cutoff frequency ω_{ct} would cause a magnetic flux $B_{\mathrm{m,HF}}(t)$ in the core that is compensated by the high-frequency current flowing in the burden winding and through the burden resistor R_{B}. Due to the core material's high permeability, the resulting magnetizing flux density is very small at these frequencies and ideally, no signal will be measured by the flux sensor. On the other hand, any frequency components $i_{\mathrm{m,LF}}(t)$ that are below the CT's lower cutoff frequency ω_{ct} would, in a first approximation, not induce a voltage in the burden winding. However, they are captured by the flux sensor and therefore, the amplifier will drive a compensating current in the burden winding, allowing a measurement with a bandwidth ranging from DC to several megahertz. As a result, the total flux density in the transformer core is close to zero over the whole frequency range of the sensor. Therefore, this concept is sometimes referred to as *zero-flux* type sensor [11].

Note that the current used to compensate the low-frequency flux is fed directly into the burden winding. Therefore, the voltage $v_{\mathrm{m}}(t)$ across the burden resistor is directly proportional to the measured current $i_{\mathrm{m}}(t)$. Unlike with open-loop sensors,

no signal processing stage is required to add the separate low- and high-frequency measurement signals.

Compared with an open-loop system, closed-loop sensors are less susceptive to gain variation of the flux sensor because the core flux density is close to zero at all times. Additionally, they show a better linearity because the flux density in the core is close to zero independently of the measured current. This avoids the nonlinearity introduced by the core material in open-loop systems. However, these advantages come at the cost of an additional analog amplifier, which is required to drive the compensation current.

As described in the earlier section and as shown in [11] and [12], no precise matching between the frequency responses of the CT and the flux sensor is required. To achieve a flat frequency response in the closed-loop system, it is sufficient to employ a flux sensor with an upper cutoff frequency well above the CT's lower cutoff frequency ω_{ct}.

E. Flux Sensing Techniques

Clearly, the flux sensor is a key component for open- and closed-loop isolated current sensors. Several flux sensing techniques are used in industrial sensors; the most common commercial sensors are based on the magnetoresistive effect, the Hall effect, and the magnetooptical effect, or make use of the magnetic saturation effects.

Magnetoresistive sensors are based on the phenomenon that certain materials exhibit a change in electrical resistance in the presence of a magnetic field [13]. While no transformer is required to implement a current sensor based on the magnetoresistive effect, it is highly nonlinear and temperature dependent. Therefore, active compensation using linear amplifiers and complex trimming schemes are required [14].

Hall-effect-based sensors come in a number of varieties and can be operated with or without a magnetic core. Versions employing a core may use flux compensation windings to improve linearity and bandwidth [1]. However, if a core is used, a gap is required to insert the sensor into the magnetic path for measuring the flux density within the core. This reduces the magnetizing inductance of the CT formed by the compensation winding, which compromises its lower cutoff frequency ω_{ct} and hence increases the required Hall effect sensor bandwidth.

Magnetooptical current sensors exploit the *Faraday effect* and are usually applied in high-current applications [15]. The glass fiber typically used as primary sensing element provides inherent isolation up to several kilovolts or more. However, optical equipment such as lasers, polarization filters, and lenses, are required. Additionally, these sensors can be susceptible to magnetic fields caused by conductors running near the line to be measured.

Furthermore, there are several methods involving a saturable magnetic material in order to measure a current. Sensors of this kind, often called flux gates, are similar to regular CTs. However, they periodically saturate the transformer's soft magnetic core. As a consequence, different effects related to the transformer's saturation can be evaluated by means of analog or digital signal processing in order to reconstruct the amplitude of the DC flux inside the core [16], [17]. Typically, very high sensitivities and linearities can be reached with these sensors [18]. Current sensors based on flux gates can be operated in open-loop or closed-loop systems and may require more than one magnetic core to improve accuracy and bandwidth and to reduce disturbances caused by the periodic saturation of the core [17].

In [19], a current sensor based on inverse magnetostriction has been presented. Inverse magnetostriction describes the change of permeability of ferromagnetic material when a mechanical strain is applied. The authors use a ferromagnetic core, which is strained by a piezoelectric actuator that causes a change of its magnetic properties. This induces a voltage in a pick-up coil wound around the core. No closed-loop compensation is applied. Several gaps are cut into the core to reduce hysteresis and to expand the dynamic range of the sensor.

In this paper, a new flux measurement concept based on magnetostriction is proposed. Its feasibility is demonstrated in the application of an isolated current measurement system providing a wide bandwidth and a large measurement range.

In Section II, the operation principle and the theoretical background of the new technique are presented. In order to demonstrate the concept's feasibility, a prototype system capable of measuring ± 20 A has been implemented. The design procedure and the major component selection for the prototype system are presented in Section III. Measurement results comparing it with commercial current sensors are given in Section IV.

II. Theory of Operation

The proposed DC + AC current sensor is based on a closed-loop compensated CT, as introduced in Section I-D. A novel principle, based on magnetostriction, is used to measure the core flux. Magnetostriction is the relative change in length of a ferromagnetic material under the presence of a magnetic field. It will be shown that this change in length of a magnetic core, measured at its surface, allows the derivation of the sign and magnitude of the magnetic flux density within the core.

Unlike current sensors based on other types of flux sensors such as Hall elements, this system does not require any gap in the magnetic path in order to insert the sensor. Therefore, the core can be operated as a transformer with a high magnetizing inductance, while at the same time, it is still possible to measure and compensate the flux components below the transformer's cutoff frequency by measuring the magnetostriction on the core's surface.

A. Magnetostriction-Based Flux Sensing

Magnetostriction is the relative change in length $\Delta l/l$ of a magnetic material when a magnetic flux density B is applied. This change of length can be measured on the surface of the core; hence, no gap is required to insert the sensor into the magnetic path. This implies that cores without a gap, e.g., toroidal cores, can be used without any modification.

As described in [20] and [21], the relative change in length $\Delta l/l$ caused by magnetostriction is, in a first approximation, proportional to the square of the magnetic flux density B for values much smaller than the saturation flux density B_{S}. The link between flux density and the relative change in length

is typically given as saturation magnetostriction λ_S, which describes the relative change in length reached at saturation flux density, as shown in the following:

$$\frac{\Delta l}{l}(B) \approx B^2 \cdot \frac{\lambda_S}{B_S^2} \quad \text{for} \quad B \ll B_S. \tag{1}$$

The saturation magnetostriction λ_S is a characteristic parameter of a ferromagnetic material and can be either positive or negative depending on the material. A value of approximately ± 15 µm m^{-1} is typically found for grain-oriented electrical steel [21]. The amorphous-iron-based alloy *2605SA1* from *Hitachi Metals/Metglas*, which is used in the prototype system has a specified saturation magnetostriction of $\lambda_S = 27$ µm m^{-1}.

The magnetostrictive strain can be measured with an electromechanical transducer, which converts the change in length to an electrical signal. Possible electromechanical transducers include strain gauges and piezoelectric sensors. A strain gauge changes its electric resistance depending on the applied elongation. The sensitivity of metallic foil strain gauges is typically around 2 mV/µm m^{-1}. As strain gauges are powered by an external supply voltage, elongations constant in time can be captured. Piezoelectric transducers, on the other hand, feature an inherent high-pass characteristic with a cutoff frequency of typically $10 \ldots 100$ Hz. Consequently, only periodic elongation variations, caused by AC flux signals, can be measured using piezoelectric sensors. Therefore, a special modulation technique is required in order to use a piezoelectric sensor for measuring DC flux densities. Advantageously, piezoelectric sensors with sensitivities of approximately 20 mV/µm m^{-1}, ten times higher than that of strain gauges, are available.

Due to the dependence on B^2 in (1), a direct measurement of the transformer core's change in length $\Delta l/l$ results in a nonlinear sensor output signal $v_S(t)$. In addition, the sign of the flux density and therefore the sign of the magnetization current are not preserved. This implies that the flux density cannot be driven to zero by a controller as the sign of the remaining core flux density would be required.

The aforementioned drawbacks can be overcome by injecting a sinusoidal voltage signal through an additional winding. This concept will be presented in the following.

B. AC Excitation

An additional excitation winding, connected to a sinusoidal voltage source $v_{ex}(t)$, is added to the core to create an additional sinusoidal component $B_{ex}(t) = \widehat{B}_{ex} \sin(\omega_{ex} t)$ in the core's flux density (cf. Fig. 3). Note that a sufficient impedance Z_{ex} is required in series with the voltage source $v_{ex}(t)$ to prevent it from shorting the burden resistor R_B. Furthermore, a second transformer core is required to prevent the low-impedance burden from shorting the excitation voltage source. This will be explained in more detail later.

As described in Section I-D, flux density frequency components sufficiently above the CT's lower cutoff frequency are compensated by the burden winding. Therefore, in a first approximation, only flux density components below ω_{LF}, and the excitation signal remain in the core, i.e.,

$$B(t) = B_{LF}(t) + \widehat{B}_{ex} \sin(\omega_{ex} t). \tag{2}$$

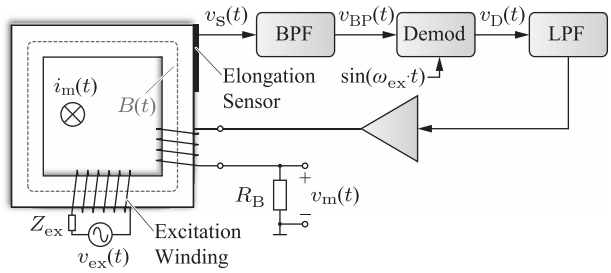

Fig. 3. Simplified block diagram of AC excitation and signal processing of the magnetostriction-based flux sensor.

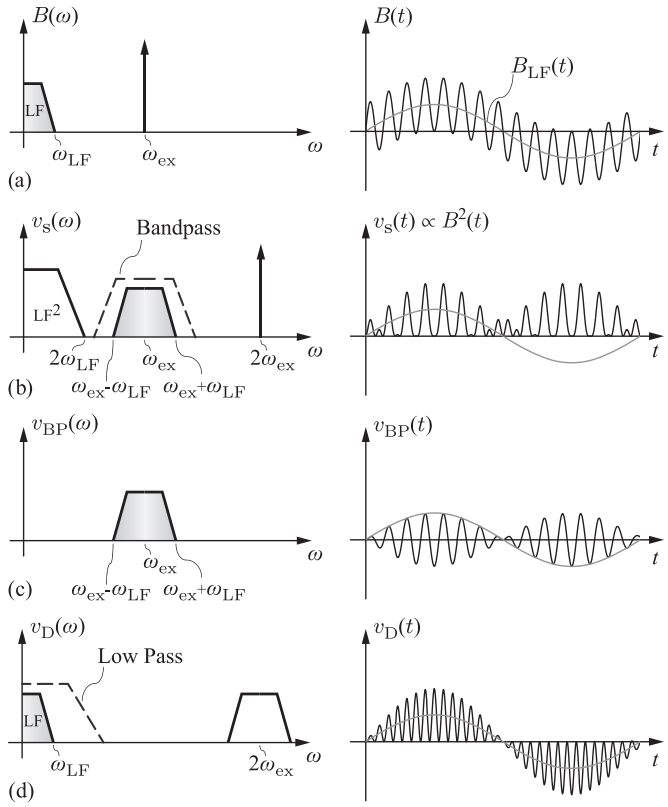

Fig. 4. Resulting spectra with AC excitation of (a) the magnetic flux, (b) the flux sensor's output signal, (c) the bandpass-filtered signal, and (d) the demodulated signal. The time-domain representation of an example signal is shown next to each spectrum for illustration.

In Fig. 4(a), the resulting spectrum of the flux density $B(t)$ is shown. Based on (1) and (2), the spectrum of the strain sensor's output signal $v_S(t)$ can be calculated as follows:

$$\begin{aligned} v_S(t) \propto B^2(t) &= \left(B_{LF}(t) + \widehat{B}_{ex} \sin(\omega_{ex} t)\right)^2 \\ &= B_{LF}^2(t) + \frac{\widehat{B}_{ex}^2}{2} + \underbrace{2 B_{LF}(t) \widehat{B}_{ex} \sin(\omega_{ex} t)}_{\text{AM Modulated Excitation}} \\ &\quad + \frac{\widehat{B}_{ex}^2}{2} \sin(2\omega_{ex} t). \end{aligned} \tag{3}$$

The resulting spectrum of the sensor's output signal is illustrated in Fig. 4(b). As shown in (3), the superposition of a sinusoidal excitation flux density $B_{ex}(t)$ and the nonlinear characteristic of magnetostriction introduce new frequency

components in the sensor's output signal. Thus, the spectrum of the sensor's signal $v_{\mathrm{s}}(t)$ differs from the spectrum of the core flux density in several aspects. A new component occurs at twice the excitation frequency $2\omega_{\mathrm{ex}}$ due to the squaring of the excitation signal $B_{\mathrm{ex}}(t)$. Furthermore, the low-frequency signal's amplitude is squared, and the bandwidth is doubled to $2\omega_{\mathrm{LF}}$. In addition, the DC value is increased by $\widehat{B}_{\mathrm{ex}}^2/2$. The most important difference, however, is the fact that the excitation frequency component is now amplitude modulated by the original low-frequency spectrum of $B_{\mathrm{LF}}(t)$. This means that a double-sided copy of the spectrum of $B_{\mathrm{LF}}(t)$ is now centered around the excitation frequency ω_{ex} [cf. middle term in (3) and Fig. 4(b)]. Note that this is in accordance with measurements published in [22].

For this reason, the modulated signal, which is purely AC, can easily be measured with a piezoelectric transducer, as long as the transducer's lower cutoff frequency is below $\omega_{\mathrm{ex}} - \omega_{\mathrm{LF}}$. In addition, based on Fig. 4(b), it can be noticed that the excitation frequency ω_{ex} has to be at least $3\omega_{\mathrm{LF}}$. Otherwise, the signal centered around the excitation frequency ω_{ex} would overlap with the spectrum of $B_{\mathrm{LF}}^2(t)$, which would result in a distortion of the original signal $B_{\mathrm{LF}}(t)$.

The amplitude-modulated excitation signal can be used to measure the low-frequency signal $B_{\mathrm{LF}}(t)$. Hence, the desired components centered around the excitation frequency ω_{ex} have to be isolated with a suitable bandpass filter (cf. Fig. 3). The spectrum of the filtered output signal $v_{\mathrm{BP}}(t)$ is shown in Fig. 4(c).

In a further step, the bandpass-filtered signal $v_{\mathrm{BP}}(t)$, which is $2B_{\mathrm{LF}}(t)\hat{B}_{\mathrm{ex}}\sin(\omega_{\mathrm{ex}}t)$, i.e., whose amplitude depends linearly on $B_{\mathrm{LF}}(t)$, can be demodulated by the multiplication with $\sin(\omega_{\mathrm{ex}}t)/\widehat{B}_{\mathrm{ex}}$. This yields the demodulator output $v_{\mathrm{D}}(t)$ containing the intended component $B_{\mathrm{LF}}(t)$, as well as a copy centered around $2\omega_{\mathrm{ex}}$ as shown in Fig. 4(d). With a subsequent low-pass filter, this copy can be rejected.

This principle allows the sensing of positive and negative magnetization currents without applying an additional offset current. Furthermore, the amplitude $\widehat{B}_{\mathrm{ex}}$ of the excitation signal gives a degree of freedom, which allows to scale the magnetostriction signal amplitude independently of the magnitude of $B_{\mathrm{LF}}(t)$. Moreover, no DC signal has to be measured by the magnetostriction sensor. This allows the usage of sensitive piezoelectric transducers, which have an inherent high-pass characteristic, and it eliminates problems with DC drifts and offsets of amplifiers in the signal path. However, the AC excitation flux in the core will induce a voltage in the burden and measurement windings and will therefore disturb the measured signal. Furthermore, the excitation source is essentially shorted by the low impedance conduction path formed by the burden winding and the burden resistor. This has to be compensated by employing a second transformer as it will be explained in the following section.

C. Compensation Transformer

The AC excitation signal introduced in the previous section creates a sinusoidal flux in the transformer core. This flux induces an excitation frequency voltage in the burden winding and the conductor carrying the measured current $i_{\mathrm{m}}(t)$. As any voltage induced in the burden winding will drive a current through the burden resistor R_{B}, a corresponding distortion of the output signal $v_{\mathrm{m}}(t)$ results. Additionally, the voltage induced in the measurement winding (carrying $i_{\mathrm{m}}(t)$) will drive a current in the circuit under test due to the circuit's impedance Z_{M}. This is far from the ideal behavior of a current sensor that should have as little influence on the circuit under test as possible.

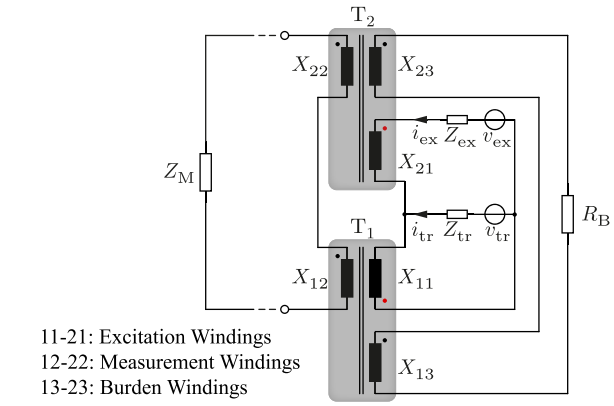

Fig. 5. Schematic representation of the current transducer comprising measurement windings, burden windings, and excitation windings. These last ones are used to inject the AC high-frequency signal and to perform the required trimming in the magnetic core.

If these disturbances in $i_{\mathrm{m}}(t)$, caused by the excitation winding, cannot be tolerated, a second transformer T_2 with the same winding arrangement as T_1 can be connected in series to it. However, the polarity of the excitation winding is reversed in T_2 (cf. Fig. 5). Consequently, in the cores of T_1 and T_2, the same AC excitation signal is impressed with the opposite sign. Assuming identical properties of the two transformers, this results in a cancelation of the voltages induced in the measurement and burden windings. Similar approaches can be found in flux gate current sensors, which are based on excited CTs as well [9].

However, due to production and assembly tolerances prevalent in a real system, the two transformers will not be exactly identical. This leads to an incomplete cancelation of the excitation signal in both the burden winding and in the measured conductor. Depending on the application of the sensor, the remaining excitation frequency disturbance might still exceed design specifications. If this is the case, it can be reduced further by introducing an additional source $v_{\mathrm{tr}}(t)$ at the connection point of the two excitation windings, which will create a corresponding trimming current $i_{\mathrm{tr}}(t)$ (cf. Fig. 5). The following section will reveal that, with this additional source, the undesired effects introduced by the nonidentical transformers can be significantly reduced.

D. Trimming

As mentioned earlier, the voltage source $v_{\mathrm{tr}}(t)$ in Fig. 5 can be used to control $i_{\mathrm{tr}}(t)$. This current allows to trim the system in such a way that undesired signals, introduced by slight differences in the transformer properties, can be minimized.

In order to analyze the resulting circuit, all other sources, i.e., the compensation voltage and the source driving the input current $i_{\mathrm{m}}(t)$, are removed. This represents a current sensor operating with zero input current and the equivalent circuit in Fig. 5 results, where Z_{M} models the impedance of the circuit that provides the current in the measurement winding.

As the excitation signal $v_{\mathrm{ex}}(t)$ creates flux densities in the cores that are sufficiently below the core material's saturation flux density, the transformers can be described by a system of linear equations. This implies that an algebraic expression for $i_{\mathrm{tr}}(t)$ can be found, which reduces the remaining current $i_{\mathrm{B}}(t)$ in the burden resistor to zero. However, this expression is rather complex as each of the two transformers T_1 and T_2 is described by three inductance values, three mutual inductance values, and three winding resistances. Together with Z_{M} and R_{B}, a system of 20 linear equations is obtained.

In order to avoid the measurement of these parameters, a numerical optimization algorithm, based on grid search with mesh refinement, is used to select the optimal amplitude and the phase angle of $i_{\mathrm{tr}}(t)$. The algorithm is executed once at the startup of the system with zero input current $i_{\mathrm{m}}(t)$. It starts by selecting an amplitude and phase angle for the trimming voltage $v_{\mathrm{tr}}(t)$, which is applied to the winding. The resulting amplitude $\hat{I}_{\mathrm{B}(\omega_{\mathrm{ex}})}$ of the excitation frequency component in the spectrum of the burden resistor current $i_{\mathrm{B}}(t)$ is measured and stored. Afterward, a new amplitude or phase angle is selected and applied, and $\hat{I}_{\mathrm{B}}(\omega_{\mathrm{ex}})$ is measured. Once a full grid pattern, covering the entire parameter space, has been sampled, the point that achieved the lowest amplitude $\hat{I}_{\mathrm{B}(\omega_{\mathrm{ex}})}$ is selected. The same procedure is then repeated with a finer grid, covering a smaller subspace in the vicinity of the selected point. This grid refinement is repeated until an amplitude and phase angle are found, which result in a sufficiently low disturbance of the burden resistor current $i_{\mathrm{B}}(t)$. The parameters achieving the lowest disturbance are then applied to the hardware and kept constant during the operation of the current sensor.[1]

Note that this algorithm can only be executed while the measured current $i_{\mathrm{m}}(t)$ is zero. Otherwise, any excitation frequency component in $i_{\mathrm{m}}(t)$ would be counteracted by $i_{\mathrm{tr}}(t)$ as the algorithm minimizes the excitation frequency component's amplitude in the output signal.

III. Design Procedure

To verify the proposed current measurement principle, a prototype has been built. It is capable of measuring currents up to ± 20 A with a bandwidth of DC to 20 MHz. This section describes the main design steps and the components selected for the prototype system. As described earlier, two magnetic cores, showing a relatively high magnetostriction, are the key components.

[1]This optimization algorithm assumes that the problem is convex, i.e., that the measured amplitude $\hat{I}_{\mathrm{B}(\omega_{\mathrm{ex}})}$ of the excitation frequency component is a convex function of the trimming voltage phase angle and amplitude. Measurements taken on a prototype system indicate that this is the case (cf. Fig. 13).

TABLE I
Tested Magnetic Materials

Type	Material	B_{sat}	v_{s} @ B_{sat}
Amorphous	2605SA1	1.56 T	94 mV
Iron Powder	MPP 160	$\approx$ 0.3 T	44 mV
Ferrite	C	0.38 T	41 mV
Ferrite	N30	0.38 T	29 mV

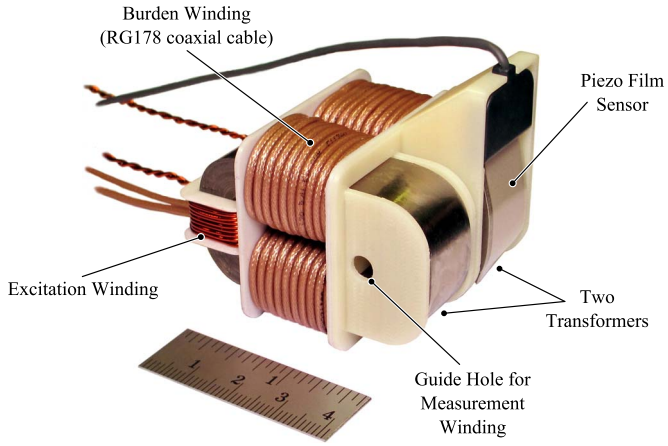

Fig. 6. CTs used in the prototype system, showing the winding arrangement and the piezo film sensor (magnetic shielding housing removed for demonstration purpose). Dimensions: $56 \times 50 \times 46$ mm ($2.2 \times 1.97 \times 1.81$ in).

A. Transformer Core

The first step in designing the CT is selecting a core material that has a sufficiently high saturation magnetostriction λ_{S} while allowing the implementation of a wideband transformer. However, magnetostriction data are typically not available in the data sheets of magnetic materials. Therefore, different materials were tested, and the measurement results are summarized in Table I. To compare the candidates, a piezoelectric sensor was attached to each sample. The cores were then magnetized using a winding connected to an AC current source. Using an oscilloscope, the amplitude of the sensor voltage at twice the excitation frequency was measured. The obtained results were then scaled to the sensor voltages expected at saturation flux density using (1).

Table I shows that the laminated amorphous material *2605SA1* from *Hitachi Metals/Metglas* has more than twice the signal amplitude compared with other materials. Hence, it was selected as core material for the prototype's CTs. With this material, the smallest commercially available core is the C-shaped *AMCC-4* (cf. Fig. 6). To demonstrate the feasibility of the concept, a relatively high cutoff frequency of $\omega_{\mathrm{ct}} \approx 2\pi \cdot 500$ Hz was selected. A smaller core, if available, would have been sufficient to implement the transformers with similar bandwidth. Note that smaller CTs with a similar current rating and bandwidth are commercially available, e.g., *Pearson 8105-03* [23].

Fig. 7 illustrates the arrangement of the individual windings on the transformer core. For the burden winding, an *RG178* coaxial cable was used in order to shield the burden winding from external electric fields. Twenty turns are used for the burden winding resulting in a lower cutoff frequency of $\omega_{\mathrm{ct}} = 2\pi \cdot 530$ Hz. Using more turns would lower ω_{ct}. However, it would

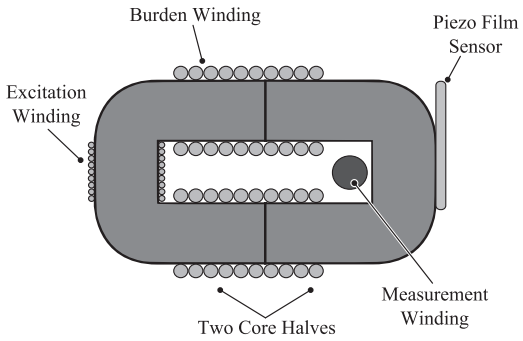

Fig. 7. Winding arrangement of one of the transformers and the placement of the piezo transducer.

TABLE II
CT PARAMETERS

Parameter	T1	T2
Core Material	Hitachi Metals 2605SA1	
Core Shape	AMCC-4 (C-shaped)	
Measurement Winding	1 Turn $0.75\,\mathrm{mm}^2$ round Cu Wire	
Burden Winding	20 Turns RG178 Coaxial Cable	
Lower CT Cut-off Frequency	$\omega_{\mathrm{ct}} = 2\pi 530\,\mathrm{Hz}$	
Upper CT Cut-off Frequency	20 MHz	
Burden Winding Resistance	$\approx 2\,\Omega$	
External Burden Resistor	$0.33\,\Omega$	
Excitation Winding	9 Turns $0.14\,\mathrm{mm}^2$ Cu Wire	
$L_{\mathrm{Measurement}}/\mu\mathrm{H}$	0.77	0.78
$L_{\mathrm{Burden}}/\mu\mathrm{H}$	297	302.8
$L_{\mathrm{Excitation}}/\mu\mathrm{H}$	64.6	64.3
$k_{\mathrm{Measurement-Burden}}$	0.855 - 0.92	0.858 - 0.914
$k_{\mathrm{Measurement-Excitation}}$	0.83 - 0.92	0.849 - 0.927
$k_{\mathrm{Burden-Excitation}}$	0.924	0.927

also potentially degrade the transformer's high-frequency performance due to the increased winding capacitance. With this winding arrangement and a burden resistor of 0.33 Ω, the CT's upper cutoff frequency was determined to be 20 MHz using a network analyzer. The number of turns required for the excitation winding is discussed in Section III-C. Table II lists the measured properties of the two transformers, whereas k_{xy} is the coupling factor between windings x and y, defined by

$$k_{\mathrm{xy}} = \frac{L_{\mathrm{xy}}}{\sqrt{L_{\mathrm{x}} L_{\mathrm{y}}}}. \tag{4}$$

L_{xy} is the mutual inductance between windings x and y and L_{x} is the self-inductance of winding x. An ideal transformer has coupling factors of 1. The coupling factors related to the measurement winding depend on the position of the measurement winding within the transformer and its length. As long as the winding arrangement is similar for both transformers, the coupling factors are almost identical and, as a consequence, so are the mutual inductances.

B. Piezo Film Sensor

As described in Section II-A, the piezoelectric strain sensor with sensitivities about ten times higher than metallic foil strain gauges are commercially available. An *SDT1-028k* piezoelectric film sensor from *Measurement Specialities* was selected for the prototype because the sensor element and the terminal wires

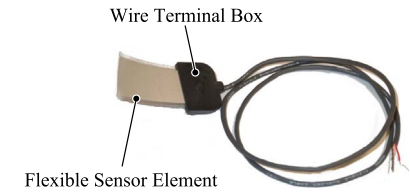

Fig. 8. *SDT1-028k* piezo film sensor where the sensor element, the terminal box, and the signal wire are electrically shielded.

are electrically shielded. This reduces electrical interference to the sensor output. Fig. 8 shows a picture of the sensor, which is approximately 30 mm long and has a nominal sensitivity of 15 $\mathrm{mV}/\mu\mathrm{m\ m}^{-1}$. Further information can be found in the sensor's data sheet [24].

As the sensor measures a mechanical strain, it is important to isolate it from external mechanical influences such as vibrations that might generate erroneous sensor signals. Therefore, a solid magnetic core without a gap is preferable since it eliminates mechanical vibrations that might arise from the contacting core halves. Additionally, as the sensor itself is not shielded against magnetic fields, care must be taken in order to avoid the generation of erroneous sensor output signals due to stray magnetic fields of the CT windings. In the prototype, the sensor was placed inside a magnetic shielding housing to mitigate the stray field sensitivity.

The sensor was adhered to one of the two transformer cores using cyanoacrylate as recommended in the *SDT1-028k*'s data sheet. In this case, the operating temperature range is limited by the sensor to 0 °C–70 °C. Sensors with a wider temperature range are available from the same vendor upon request.

C. Excitation and Trimming

The next step in the design procedure is the selection of the excitation frequency ω_{ex}. As explained in Section II-B, the excitation frequency has to be at least three times the frequency of the highest spectral component (ω_{LF}) of the core flux density B_{LF} to be measured. As an approximation, ω_{LF} is assumed ten times the CT's cutoff frequency ω_{ct}. Therefore, an excitation frequency $\omega_{\mathrm{ex}} = 2\pi \cdot 16\ \mathrm{kHz} \approx 3 \cdot 10 \cdot \omega_{\mathrm{ct}}$ was selected. Selecting higher excitation frequencies would not improve the performance significantly but would increase the core losses in the transformers and hence increase the power consumption of the system.

A further tradeoff exists between core losses and the excitation flux density amplitude $\hat{B}_{\mathrm{ex}}$. The signal amplitude of the piezoelectric sensor, and hence the sensitivity of the magnetizing current measurement, increases with $\hat{B}_{\mathrm{ex}}$. However, the core losses of the transformers increase as well. A peak excitation flux density of $\hat{B}_{\mathrm{ex}} \approx 45$ mT was selected for the prototype system. Note that this is well below the material's saturation flux density of 1.56 T.

Once the required excitation flux density is defined, the excitation and trimming voltage amplifiers can be designed. Operational amplifiers were used to implement the excitation and trimming sources. The selected components are listed in Table III. Note that the excitation winding's number of turns

TABLE III
EXCITATION AND TRIMMING PARAMETERS

Number of Turns	$N_{\rm ex}$	9
Excitation Amplifier		*TCA0372*
Excitation Source Impedance	$Z_{\rm ex}$	33 µH
Excitation Voltage	$\hat{v}_{ex}$	10 V
Excitation Current	$\hat{i}_{ex}$	350 mA
Trimming Amplifier		*TCA0372*
Trimming Source Impedance	$Z_{\rm tr}$	39 Ω & 100 µH
Trimming Voltage	$\hat{v}_{tr}$	6 V
Trimming Current	$\hat{i}_{tr}$	50 mA

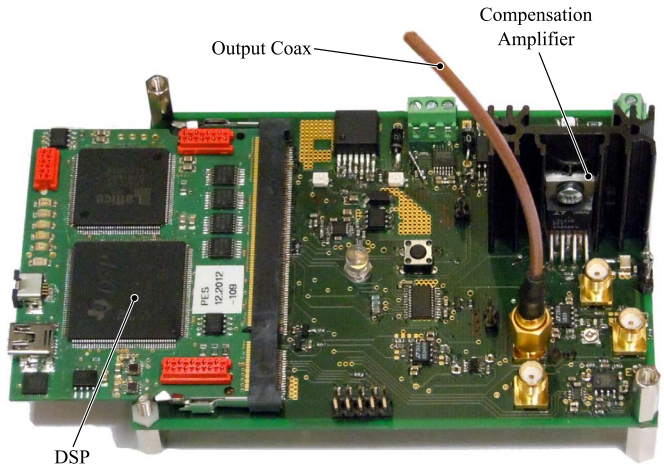

Fig. 9. Analog and digital circuits of the prototype system utilized for signal processing. Miniaturization of the circuitry was not an implementation target due to the prototyping nature of the system. Dimensions: 135 × 80 mm (5.3 × 3.1 in).

$N_{\rm ex}$ can be used to select the voltage required by the excitation voltage source, i.e.,

$$\hat{v}_{\rm ex} > 2 \cdot \hat{B}_{\rm ex} \cdot A_{\rm e} \cdot N_{\rm ex} \cdot \omega_{\rm ex}. \tag{5}$$

D. Signal Processing

A digital signal processor handles the signal generation, filtering, demodulation, flux control, measurement routines, and trimming. The analog and digital circuitry built for the prototype system is shown in Fig. 9. The two filters shown in Fig. 3 are implemented as digital filters. The bandpass is a tenth-order Chebyshev Type 2 filter with a passband of 11–21 kHz providing 50 dB attenuation for frequencies below 7 kHz and above 33 kHz. The low pass is a fourth-order Chebyshev Type 2 filter with 1-dB attenuation at 10 kHz and 50 dB attenuation above 32 kHz. A proportional–integral (PI) controller is used as a flux controller.

IV. MEASUREMENT RESULTS

A. Magnetizing Current Measurement

To verify that the magnetostriction-based flux sensor is able to measure the CT's magnetizing current, the step response of the uncompensated system has been measured. Fig. 10 shows measurement results obtained from the specified prototype system. Initially, the CT's output signal $i'_{\rm B}$ follows the rising

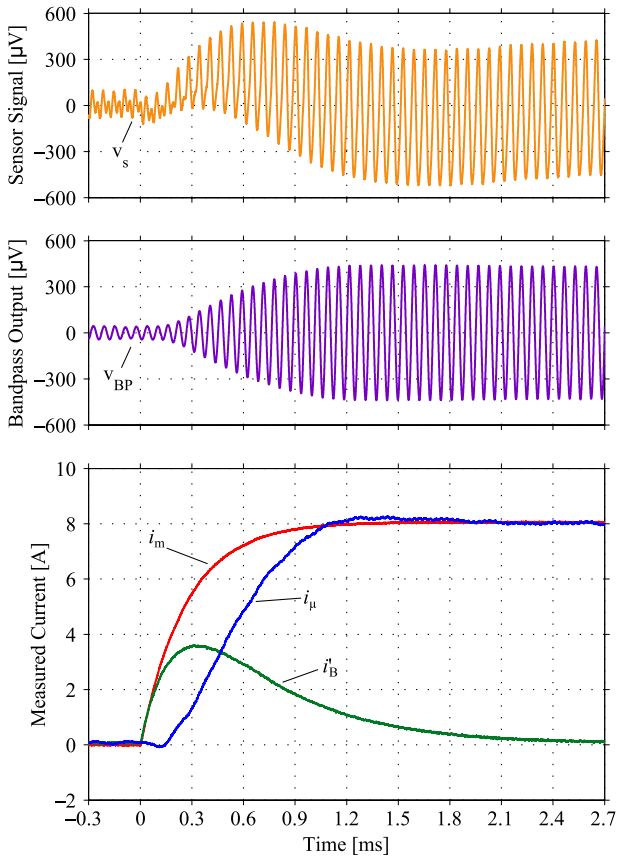

Fig. 10. Plot of the system's response to an 8-A current step in open-loop operation, i.e., with compensation turned off. Initially, the sensors output $i'_{\rm B}$ tracks the current to be measured $i_{\rm m}$. Due to the voltage drop across the burden, the magnetizing current of the transformer increases; hence, the output signal drops to almost zero. At the same time, the amplitude of the signal $v_{\rm s}$ measured by the piezo sensor increases. After bandpass filtering ($v_{\rm BP}$), only the amplitude modulated excitation frequency signal remains. Demodulation and low-pass filtering of $v_{\rm BP}$ yields the magnetizing current i_{μ}.

current $i_{\rm m}$. However, due to the CT's high-pass characteristic ($\omega_{\rm ct} = 530$ Hz), $i'_{\rm B}$ decays towards zero, which implies that a magnetizing current starts to flow. As a consequence, the amplitude of the excitation frequency signal increases in the piezo sensor's output signal $v_{\rm S}$, as shown in the top plot. As expected, the sensor's output signal contains further spectral components, which are removed by the bandpass filter. Therefore, an amplitude modulated, sinusoidal signal $v_{\rm BP}$ with excitation frequency remains after the bandpass filter. Demodulation and rescaling of $v_{\rm BP}$ yields the magnetizing current signal i_{μ}.

B. Dynamic Performance

To verify the closed-loop performance of the prototype, it has been compared with two commercially available clip-on current probes which have bandwidths of 50 MHz (*Ref 1*) and 100 MHz (*Ref 2*), respectively and are designed to be used with oscilloscopes. In Fig. 11, the response to a 17 A current step is shown. Note that the current pulse is long enough that both, the CT and the flux compensation circuit, are involved in the current measurement. The output signal of the device under test (DUT) matches the measurement of the two reference current probes.

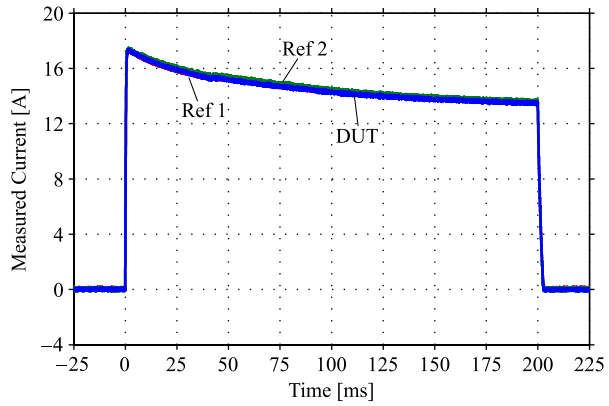

Fig. 11. Response to a 17 A current step. In this test, both the flux measurement concept and the CT are utilized. During the initial step, the CT is active, whereas during the decaying current ramp, the flux sensor is providing the information for the sensor's output.

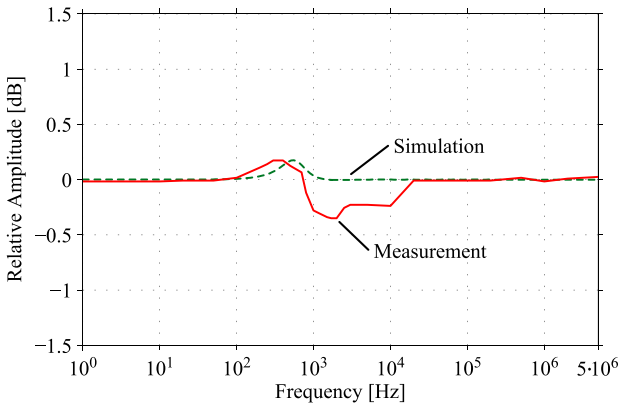

Fig. 12. Amplitude response of the closed-loop system. The maximum deviation occurs at 2 kHz and has a magnitude of 0.35 dB, which corresponds to an error of 4.1%. This is the same order of magnitude, which is specified for the current probes used as reference.

Furthermore, the prototype's amplitude response is shown in Fig. 12. A sinusoidal current source was used to create a test signal of varying frequency. Fig. 12 shows the ratio between the signal amplitudes measured by the DUT and *Ref 1*. A positive deviation of ≈ 0.2 dB exists around 500 Hz, which is where the compensation performed by the flux sensor, and the PI controller ends and the CT takes over. This is in good accordance with a simulated frequency response of the system as shown. Another deviation from the ideal value of 0 dB occurs around ≈ 2 kHz. This deviation could be the result of an unknown nonlinearity and/or analog signal coupling that disturbs the system. A detailed analysis is relatively extensive and out of the scope of the paper, which is focused on the analysis and verification of a new flux density measurement principle. However, the deviation's magnitude is less than 0.35 dB, which corresponds to an error of 4.1%. This is comparable to the accuracy values of the reference probes.

C. Excitation Voltage Trimming

As described in Section II-D, a trimming scheme is used to minimize the disturbance on the sensor's output signal caused by small differences of the transformer cores and the excitation

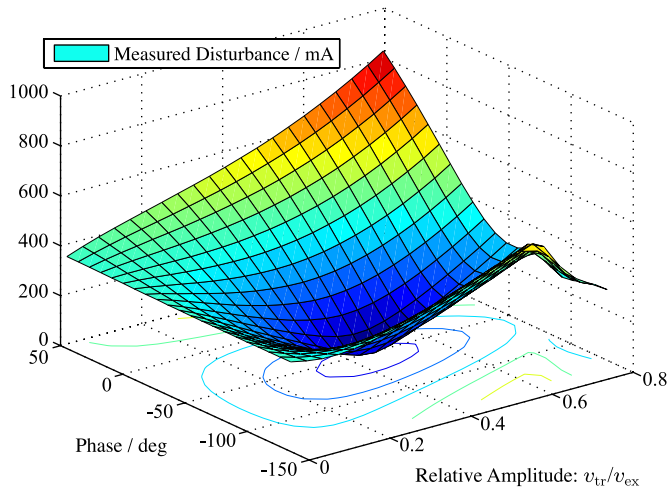

Fig. 13. Excitation frequency disturbance in the output signal $v_m(t)$ as function of trimming voltage with zero input current i_m applied. The bend in the plot, for relative amplitudes > 0.6 and phase angles $> -100°$, results from an unstable amplifier that was not designed for operation in this region.

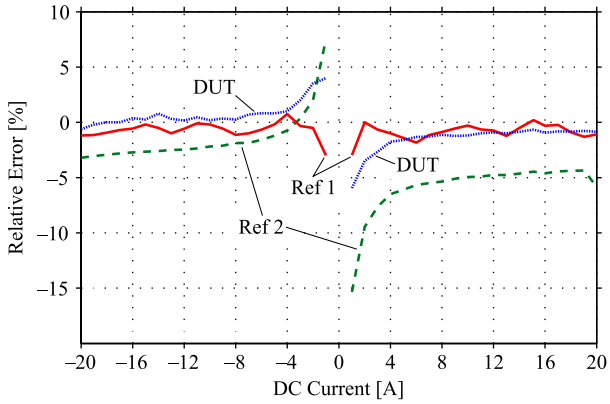

Fig. 14. Comparison of relative measurement errors with two commercial current probes, which have bandwidths in excess of 50 MHz and are designed for the use with oscilloscopes.

signal. A measurement from the prototype showing the measured excitation frequency component on the output signal as a function of trimming current phase and amplitude is given in Fig. 13. In the prototype, the trimming source is implemented as a voltage source with a defined series impedance. Note that there is a single minimum point where the excitation frequency component is reduced to a value that is well below the sensor's full scale output of 20 A. This point is found and selected by the algorithm described in Section II-D, which achieved a remaining distortion of the output signal corresponding to a measured current of < 4.5 mA, i.e., $< 0.023\%$ of full scale.

D. DC Precision

Additionally, Fig. 14 shows the relative measurement errors of the three current probes for DC currents from -20 to 20 A at room temperature. A *Yokogawa WT3000* precision power analyzer, with a maximum error of ± 2 mA over the full range, was used as reference. The same data were used to derive the linearity properties of all three probes. Least squares

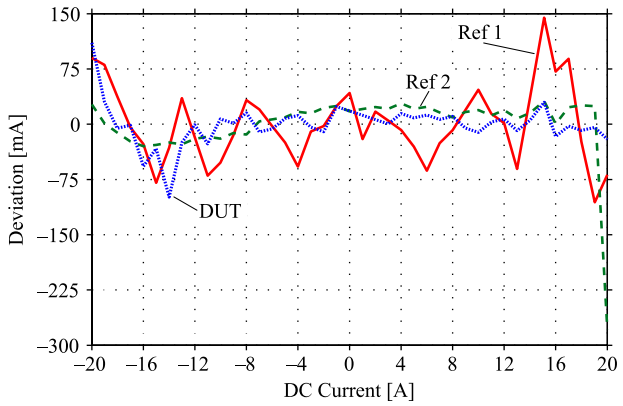

Fig. 15. Deviation of the measurement from its best linear fit for different DC values and current probes from two different manufacturers. The nominal DC ranges are ±30 A for *Ref 1* and ±20 A for *Ref 2*.

TABLE IV
LINEARITY MEASUREMENT RESULTS

Probe	Best-Fit INL	Gain Error	Offset
Ref 1	145 mA	−0.74 %	−2 mA
Ref 2	279 mA	−3.77 %	−138 mA
DUT	126 mA	−0.41 %	−68 mA

regression was used to determine the best-fit line for each probe. Fig. 15 shows the difference between the measured current and the best-fit lines of the probes. The best-fit integral nonlinearity (INL), defined as the maximum deviation between the measured value and the best-fit line, is given in Table IV.

V. CONCLUSION

This paper has presented a magnetic flux sensing principle based on the measurement of the ferromagnetic material's magnetostrictive strain. In order to detect these length changes, a piezoelectric transducer was attached to the surface of a magnetic core. Unlike other flux sensing techniques, no gap is required in the material. In addition, an AC flux signal was injected through an additional winding in order to shift the sensor's output voltage spectrum to higher frequencies, thus enabling the utilization of the piezoelectric sensor.

In order to demonstrate the technique and to prove its feasibility, a DC + AC current sensor has been implemented. Based on a closed-loop design comprising a piezoelectric sensor and the appropriate analog and digital circuitry, the accurate measurement of currents up to ±20 A from DC to 20 MHz is achieved. For DC, an INL error of less than 126 mA (0.63% full scale) is shown. These performance figures are comparable to commercial clip-on current probes for oscilloscopes, although the prototype system was not optimized for small size. The overall volume of the CTs and the signal processing PCB is $\approx 290\ \text{cm}^3$ which is comparable to *Ref 1*'s volume of $224\ \text{cm}^3$.

The presented principle is not limited to current sensing since it can potentially be applied in a wider range of applications where a DC or low-frequency magnetic flux has to be detected in a ferromagnetic material. Since there is no necessity for an air gap in the magnetic core, this technique provides a noninvasive type of flux measurement. This could be beneficial, for example, in isolated DC–DC converters. As described in [25], these converters may require some form of transformer core flux measurement in order to prevent a saturation of the core. The technique described in this paper can be used to accomplish this. As the transformer is already excited by the DC–DC converter, no additional excitation winding is needed. Therefore, only a piezoelectric sensor measuring the core's magnetostriction and analog amplifiers are required. This implies that, unlike other techniques, no modifications of the converter's circuit topology and of the transformer are required. In particular, no additional components carrying the transformer current are needed, which might result in lower losses as compared to other techniques.

REFERENCES

[1] S. Ziegler, R. C. Woodward, H. H.-C. Iu, and L. J. Borle, "Current sensing techniques: A review," *IEEE Sensors J.*, vol. 9, no. 4, pp. 354–376, Apr. 2009.
[2] C. M. Johnson and P. R. Palmer, "Current measurement using compensated coaxial shunts," *Proc. Inst. Elect. Eng.—Sci., Meas. Technol.*, vol. 141, no. 6, pp. 471–480, Nov. 1994.
[3] W. F. Ray and C. R. Hewson, "High performance Rogowski current transducers," in *Conf. Rec. IEEE IAS Annu. Meeting*, Rome, Italy, Oct. 2000, vol. 5, pp. 3083–3090.
[4] F. Costa, E. Laboure, F. Forest, and C. Gautier, "Wide bandwidth, large AC current probe for power electronics and EMI measurements," *IEEE Trans. Ind. Electron.*, vol. 44, no. 4, pp. 502–511, Aug. 1997.
[5] L. A. Kojovic, M. T. Bishop, and D. Sharma, "Innovative differential protection of power transformers using low-energy current sensors," *IEEE Trans. Ind. Appl.*, vol. 49, no. 5, pp. 1971–1978, Sep./Oct. 2013.
[6] T. Smith and R. Hunt, "Current transformer saturation effects on coordinating time interval," *IEEE Trans. Ind. Appl.*, vol. 49, no. 2, pp. 825–831, Mar./Apr. 2013.
[7] M. Rigoni *et al.*, "Rogowski coil current meters in nonconventional applications," *IEEE Potentials*, vol. 27, no. 4, pp. 40–45, 2008.
[8] L. Dalessandro, N. Karrer, and J. W. Kolar, "High-performance planar isolated current sensor for power electronics applications," *IEEE Trans. Power Electron.*, vol. 22, no. 5, pp. 1682–1692, Sep. 2007.
[9] "Isolated current and voltage transducers (3rd ed.)," LEM Components, Plan-les-Ouates, Switzerland, CH24101, 2004.
[10] J. R. Leehey, L. Kushner, and W. S. Brown, "DC current transformer," in *Proc. 13th IEEE PESC*, Cambridge, MA, USA, Jun. 1982, pp. 438–444.
[11] Y. Suzuki, A. Hirabayashi, and K. Yamasawa, "Analysis of a zero-flux type current sensor," *IEEE Trans. Magn.*, vol. 29, no. 6, pp. 3183–3185, Nov. 1993.
[12] J. A. Carrasco, E. Sanchis-Kilders, D. Ramirez, and E. J. Dede, "Improved magnetic coupled current sensing techniques," in *Proc. 27th Annu. IEEE PESC*, Jun. 1996, vol. 1, pp. 829–834.
[13] P. E. Schneider, M. Horio, and R. D. Lorenz, "Evaluation of point field sensing in IGBT modules for high-bandwidth current measurement," *IEEE Trans. Ind. Appl.*, vol. 49, no. 3, pp. 1430–1437, May/Jun. 2013.
[14] G. Laimer and J. W. Kolar, "Design and experimental analysis of a DC to 1 MHz closed loop magnetoresistive current sensor," in *Proc. IEEE APEC Expo.*, Austin, TX, USA, Mar. 2005, vol. 2, pp. 1288–1292.
[15] A. Papp and H. Harms, "Magnetooptical current transformer. 1: Principles," *Appl. Opt.*, vol. 19, no. 22, pp. 3729–3734, Nov. 1980.
[16] A. Gytri and T. M. Undeland, "Low cost DC and AC current transducer with isolation and good linearity," in *Proc. 4th Annu. Int. PCI Conf.*, Mar. 1982, pp. 341–353.
[17] P. Ripka, "Review of fluxgate sensors," *Sens. Actuators A, Phys.*, vol. 33, no. 4, pp. 129–141, Jun. 1992.
[18] Current Transducer ITZ 600-SPR Flex Ultrastab Datasheet, LEM, 2014, Accessed Jan. 2015. [Online]. Available: http://www.lem.com/docs/products/itz_600-spr_flex_ultrastab.pdf
[19] F. Koga, T. Tadatsu, J. Inoue, and I. Sasada, "A new type of current sensor based on inverse magnetostriction for large current detection," *IEEE Trans. Magn.*, vol. 45, no. 10, pp. 4506–4509, Oct. 2009.
[20] T. Zhang, C. Jiang, H. Zhang, and H. Xu, "Giant magnetostrictive actuators for active vibration control," *Smart Mater. Struct.*, vol. 13, no. 3, pp. 473–477, Jun. 2004.

[21] T. Hilgert, L. Vandevelde, and J. Melkebeek, "Comparison of magnetostriction models for use in calculations of vibrations in magnetic cores," *IEEE Trans. Magn.*, vol. 44, no. 6, pp. 874–877, Jun. 2008.
[22] Y. Ishihara, H. Maeda, K. Harada, and T. Todaka, "Performance of the magnetostriction of a silicon steel sheet with a bias field," *J. Magn. Magn. Mater.*, vol. 160, pp. 149–150, Jul. 1996.
[23] Custom Current Monitors—Model 8105-03, Pearson Electronics, Palo Alto, CA, USA, Jan. 2015. [Online]. Available: http://www.pearsonelectronics.com/products/custom-current-monitors
[24] Piezo Sensor—SDT Series, Measurement Specialties, Hampton, VA, USA, Jan. 2015. [Online]. Available: http://www.meas-spec.com/product/t_product.aspx?id=2486
[25] G. Ortiz, J. Mühlethaler, and J. W. Kolar, "'Magnetic Ear'—Based balancing of magnetic flux in high power medium frequency dual active bridge converter transformer cores," in *Proc. 8th IEEE Int. Conf. Power Electron./ECCE*, Jeju, Korea, May 2011, pp. 1307–1314.

Lukas Schrittwieser (S'14) was born in Lower Austria in 1988. He received the M.Sc. degree in electrical engineering from the Swiss Federal Institute of Technology (ETH Zurich), Zurich, Switzerland, in 2014. He is currently working toward the Ph.D. degree at the Power Electronic Systems Laboratory, ETH, where he is working on three-phase buck-type pulsewidth-modulated rectifiers.

In his master's thesis, he realized a solid-state transformer demonstrator. In an industry internship at ABB MV Drives, Milwaukee, WI, USA, he worked on medium-voltage drives. His research interests include power electronics, energy systems, and measurement technologies.

Mario Mauerer (S'14) was born in Kusnacht, Switzerland, in 1988. He received the M.Sc. degree from the Swiss Federal Institute of Technology (ETH Zurich), Zurich, Switzerland. He is currently working toward the Ph.D. degree at the Power Electronic Systems Laboratory, ETH Zurich, where his research deals with ultra-low distortion, high-power, and highly dynamic drive systems for mechatronic actuators.

His master's thesis dealt with a solid-state transformer demonstrator. He was a Visiting Student with the National University of Singapore, Singapore. His research interests include power electronics, high-voltage technology, and signal processing and drive systems.

Dominik Bortis (S'06–M'09) received the M.Sc. degree in electrical engineering and the Ph.D. degree from the Swiss Federal Institute of Technology (ETH Zurich), Zurich, Switzerland, in 2005 and 2008, respectively.

During his studies, he majored in communication technology and automatic control engineering. After an internship with ABB Switzerland, Turgi, Switzerland, he worked during his diploma thesis with the company Levitronix. Since 2008, he has been a Postdoctoral Fellow with the Power Electronic Systems Laboratory, ETH Zurich.

Gabriel Ortiz (M'10) received the M.S. degree in electronic engineering from the Universidad Técnica Federico Santa María, Valparaíso, Chile, in 2008 and the Ph.D. degree from the Swiss Federal Institute of Technology (ETH Zurich), Zurich, Switzerland.

His master's thesis dealt with reconfiguration of regenerative and nonregenerative cascaded multilevel converters under fault condition. In 2009, he joined the Power Electronic Systems Laboratory, ETH Zurich, where he focused on solid-state transformers for future smart grid implementations and traction solutions. His Ph.D. thesis dealt with the modeling, optimization, and design of high-power DC–DC converters operated in the medium-frequency range with special attention on modeling of soft-switching processes in insulated-gate bipolar transistors and medium-frequency transformer design, topics he continued and extended during his Postdoctoral activities in 2014 in the same institute. He is currently with the ABB Corporate Research Center, Baden-Dättwil, Switzerland.

Johann W. Kolar (M'89–SM'04–F'10) received the M.Sc. and Ph.D. degree (*summa cum laude*) from the University of Technology Vienna, Vienna, Austria.

He is currently a Full Professor and the Head of the Power Electronic Systems Laboratory, Swiss Federal Institute of Technology (ETH Zurich), Zurich, Switzerland. He has proposed numerous novel pulsewidth-modulated converter topologies, and modulation and control concepts. He is the author of over 650 scientific papers published in international journals and conference proceedings and has filed more than 110 patents. His research interests include ultracompact and ultraefficient converter topologies employing the latest power semiconductor technology (SiC and GaN), solid-state transformers, power supplies on chip, and ultra high-speed and bearingless motors.

Dr. Kolar received ten IEEE TRANSACTIONS and Conference Prize Paper Awards, the IEEE Middlebrook Award, and the ETH Zurich Golden Owl Award.